Meyer-Neldel correlation in semiconductors and Mott's minimum metallic conductivity

Corneliu Popescu and Toma Stoica
Institute of Physics and Technology of Materials, Bucharest, P. O. Box MG7, Magurele, Romania
(Received 26 December 1991; revised manuscript received 27 May 1992)

The paper outlines conditions under which the statistical shift of the Fermi level within the density-of-states (DOS) distribution may result in the Meyer-Neldel correlation. Sufficient conditions have been found: (i) The DOS should have, around the Fermi level, two competing exponential slopes; (ii) The temperature range for the statistical shift should correspond to kT values higher than at least one of these two characteristic energies associated with the slopes. Under such conditions, the Fermi level is no longer the dominant energy for carrier-concentration changes. Relating the Mayer-Neldel correlation to DOS parameters is an essential step in a correct deduction of Mott's minimum-metallic-conductivity value from experiment.

I. INTRODUCTION

Over a wide range of temperature, the conductivity of intrinsic and doped amorphous hydrogenated silicon (*a*-Si:H) is thermally activated,

$$\sigma=\sigma_0\exp(-E_\sigma/kT)\ , \tag{1}$$

in which E_σ is the activation energy and σ_0 is identified with the minimum metallic conductivity σ_m defined by Mott,[1] estimated to be between 16 and 100–600 $(\Omega\,\mathrm{cm})^{-1}$, but experimentally found to be orders of magnitude different.[2–4] Many attempts have been made to explain this discrepancy by considering temperature shifts of the Fermi level and mobility edge.[5]

Additional complications in the theory arise because of the existence of an exponential correlation between σ_0 and E_σ (Refs. 6–9) of the kind established by Meyer and Neldel,[10]

$$\sigma_0=\sigma_{00}\exp(E_\sigma/kT_{\mathrm{MN}})\ . \tag{2}$$

The correlation, also known as the Meyer-Neldel rule (MNR),[9] is found in electrical-conductivity measurements, on differently doped samples, as well as among various light- and thermal-treatment induced states of the same sample. It also appears in field-effect and space-charge-limited-current measurements. The characteristic energy kT_{MN} values are rather spread out, say between 0.043 and 0.067 eV.[14]

Attempts have also bee made to explain the Meyer-Neldel correlation through a linear relation,

$$E_F(t)-E_C=E_F(0)-E_c+\gamma T\ , \tag{3}$$

in which the temperature coefficient γ incorporates effects of the Fermi-level and conduction-band-edge thermal shifts. Such an equation leads to the following interpretation for the E_0 and o_0 parameters:

$$E_\sigma=E_C-E_F(0)\ , \tag{4}$$

$$\sigma_0=\sigma_m\exp(\gamma/k)\ . \tag{5}$$

Only partial success has been achieved, especially with regard to the field-effect data,[11,12] and we will show that even this might have resulted from processing the data under the assumption that the fastest space-charge change appears around the Fermi level, whatever the temperature may be.

Full success of Eq. (3) in accounting for the MNR would mean that the temperature coefficient γ satisfies the following condition:

$$\gamma/k=\ln(\sigma_0/\sigma_m)=\ln(\sigma_{00}/\sigma_m)+E_\sigma/kT_{\mathrm{MN}}\ . \tag{6}$$

In other words, this means that the physics behind the MNR should ensure a thermal coefficient of the Fermi level which varies linearly, and with a positive slope for an electron conduction, with the associated activation energy of the conductivity.

Equation (6) implies that the thermal shift of the Fermi level should be describable by a family of curves (for various E_{F0}) of the type

$$E_F(E_{F0},T)=E_{F0}+[a+b(E_C-E_{F0})]kT\ , \tag{7}$$

with the constant parameters a and b determining the deviation of the experimental value σ_{00} from Mott's minimum metallic conductivity σ_m

$$\sigma_{00}/\sigma_m=\exp(a) \tag{8}$$

and the characteristic MN energy

$$kT_{\mathrm{MN}}=1/b\ ,\quad b>0\ . \tag{9}$$

Such a family of curves, which extend linearly down to $T=0$, for all possible E_{F0} is incompatible with a continuous density of states (DOS). But MNR should appear within a temperature range over which the Fermi-level shift is well approximated by such a family of curves. If the band-edge thermal shift is to make a contribution, it would affect only parameter a, i.e., the ratio σ_{00}/σ_m, but not the MNR slope, which is related to parameter b.

A successful Meyer-Neldel-type of description using Fermi-level statistical shift, with a plausible density of states for *a*-Si:H, has been proposed by Overhof and Beyer,[13] and subsequently refined by Overhof and Tho-

mas (OT).[14] The energy-state distribution that they use combines exponential tails of states, which extend from conduction and valence bands (with characteristic energies of about 0.026 and 0.033 eV, respectively), with peaked midgap-defect-level distributions, which extend towards bands with exponential slopes.

The numerically evaluated $E_F(E_{F0},T)$ dependencies are not linear, as given by Eq. (7), but can be satisfactorily approximated by their average slope $\gamma^*=dE_F/dT$ at T_M, the center of the (measurement) temperature range of interest,

$$E_F(T)=E_{F0}^*+\gamma^* T \ , \tag{10}$$

in which the $T=0$ extrapolation E_{F0}^* is, in some cases, substantially different from $E_{F0}=E_F(0)$, as the calculated dependencies have a vanishing slope around $T=0$, even for high average slopes γ^*.

Equation (10) leads to a temperature dependence of the conductivity,

$$\sigma(T)=\sigma_0^* \exp(-E_\sigma^*/kT) \ , \tag{11}$$

with the activation energy and preexponential factor given, respectively, by

$$E_\sigma^*=E_C-E_{F0}^* \quad \text{and} \quad \sigma_0^*=\sigma_m \exp(\gamma^*/k) \ . \tag{12}$$

The calculated σ^*/k dependence on E_σ^*,[14] shown in Fig. 1, has a positive slope range within which it is approximated by the required MNR dependence as given by Eqs. (6) and (7), and can fit experimental MN correlations over about five orders of magnitude in $\sigma_0(E_\sigma)$.

The statistical-shift interpretation of MNR was called into question by Irsigler, Wagner, and Dunstan[15] because a specific density-of-states distribution was used in the above-mentioned calculations, which seemed to contradict the finding of the ubiquitous presence of the MNR.

Overhof and Thomas claim that their successful density of states is not a singular one, that reasonable $\gamma^*(E_\sigma^*)$ dependencies result for various profiles of deep-level states (even completely flat ones), and that such dependencies are a consequence of a sufficiently high ratio between band- and midgap-state densities.[14] But it remains an open question whether this is the only condition.

Moreover, even if the OT theory of the Meyer-Neldel correlation, based on numerical calculations covering a wide range of parameters, were convincing, it would still leave open several questions of even wider interest than MNR itself. First of all, there is the interpretation of the activation energies E_σ^* which are significantly different from $E_C-E_F(0)$. Then there is the problem of the dependence, between the experimentally determined σ_{00} value and Mott's minimum metallic conductivity. As Eqs. (6)–(8) and Fig. 1 suggest, the ratio σ_{00}/σ_m depends on DOS parameters that control the extent of the MNR.

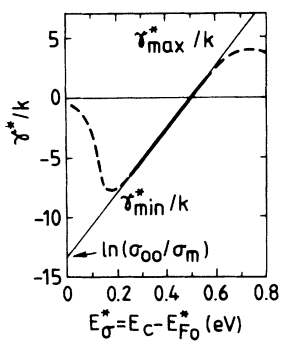

FIG. 1. γ^*/k dependence on E_σ^*.

In trying to answer these questions, we present, in what follows, results of a combined numeric and analytic treatment of the Fermi-level statistical shift, for fast-varying energy-state profiles.

Section II considers the statistical shift of the Fermi level within a DOS that has the essential features of the OT DOS, and for which MNR is obtained by a fully numerical evaluation of the shift. At the same time this DOS allows for analytic treatment and approximations which reveal the physics behind the MNR. Section III quantitatively relates the MNR to DOS parameters, and considers implications of the MNR.

II. THE THERMAL SHIFT OF THE FERMI LEVEL

As is generally known, the thermal shift of the characteristic energy of the occupancy function, i.e., the Fermi level in thermal equilibrium, is given by a charge-conservation equation which, in thermal equilibrium, is a neutrality equation, with the Fermi-Dirac occupancy function $f((E-E_F)/kT)$:

$$G(E_F)=\int_{-\infty}^{+\infty} N(E)[f((E-E_F)/kT) - \Theta(E_{F0}-E)]dE=0 \ , \tag{13}$$

in which $N(E)$ is the DOS function and $\Theta(x)$ is the Heavyside unit-step function. For a given $N(E)$, a numerical procedure combines numerical integration with a root-finder procedure for a solution of Eq. (13).

In order to resolve fully the issues raised by Irsigler, Wagner, and Dunstan, the exponential profile defined by Eq. (A1)–(A4) and Fig. 7 in Appendix A has been used. It retains the essential features of the OT DOS, i.e., disorder tails of states fast (exponentially) falling from the bands, and midgap defect states with various profiles, from peaked to flat ones.

The essential model parameters to be kept in mind for MNR analysis, in the electron conduction case, are the following: (i) the characteristic energies (related to logarithmic slopes) of the tail and midgap states, on the conduction-band side, which we assign for convenience to $t_c=kT_c$ and $m_c=kT_{mc}$, respectively; (ii) the transition energy E_{mc}, from tail to midgap defect states, on the conduction-band side (conduction-band edge E_C taken as reference); (iii) the midgap peak position E_M, if any (with respect to E_C). The extent of a flat defect-states profile is insignificant, as long as its limit is not reached in the temperature range of interest; (iv) the corresponding parameters on the valence-band side, indexed with v instead of c, are insignificant for the MNR analysis, as will be further discussed.

This DOS profile, which allowed us to make an analytic treatment, has been explored with the full Fermi-Dirac function, as well as with two-term and Boltzmann approximations, Eqs. (A5)–(A7), in Appendix A. A fully numerical procedure, with use of the Fermi-Dirac occupancy function, has shown that even for a symmetrical DOS profile, with conduction- and valence-band characteristic energies t_c, t_v of 0.026 eV, all OT results can be reproduced in the temperature range between 240 and 360 K, and for defect distributions characterized as follows: (i) tail-defect transition energies E_{mc}, E_{mv} within 0.4–0.6 eV of the respective bands, i.e., a transition at localized-state densities between 2×10^{15} and 10^{12} $cm^{-3}eV^{-1}$, for band densities of 10^{22} $cm^{-3}eV^{-1}$; (ii) characteristic energies m_c, m_v for the midgap states within the range of -0.026 eV and infinite (flat defect-states profile).

The effect of occupancy-function approximations has been further assessed, for the two-term approximation (which ensures the right value and slope at E_F as well as far from it) and for the Boltzmann approximation, valid sufficiently far above or under E_F. Details about their implications on the computational procedure are given in Appendix A.

It has been found that, for the above-mentioned temperature range in which MNR is obtained, the results do not change appreciably for these two approximations. It will be further shown that the surprisingly good performance of the crude Boltzmann approximation may be ascribed to the physics of the MNR itself.

As discussed in Appendix A, when the DOS in Fig. 7 is used in Eq. (13), the latter can be analytically integrated, and a number of exponential terms results, corresponding to the limits of the various exponential regions. These terms correspond to the space charge accumulated in various regions of the DOS, with respect to the 0-K case, while the overall neutrality is conserved, and secured through a corresponding shift of the Fermi level.

A qualitative examination of the various terms shows that, within the charge balance determining the Fermi-level position, besides the region close to this level, a significant contribution comes only from the states in the vicinity of the band edges E_C, E_V and the midgap peak E_M (if any). For the Boltzmann approximation of the occupancy function, Eq. (13) reduces to only five significant terms, Eqs. (A8)–(13) in Appendix A. Using a root finder for such a simple equation, one obtains Fermi-level-shift curves that are very good approximations of the ones obtained by using the full numerical procedure, as shown in Fig. 2. And this happens over a much wider temperature range than that of interest from the narrower perspective of the MNR.

Moreover, even when our interest was restricted to the temperature range relevant to the MNR, we found that only three-space-charge terms in Eq. (A8) remain quantitatively significant. For this temperature range, with the Fermi level on one side of the midgap peak, the terms corresponding to the space charge on the other side of the peak are negligible.

As shown in Appendix A, for the three-term equation, the root-finder procedure for obtaining E_F can be replaced with a straightforward iterative procedure, or even an explicit approximate equation, Eqs. (A15)–(A18). Figure 2 also shows the success of the three-term approximations for describing the Fermi-level thermal shift in the temperature range of relevance to the MNR, which is generally about 240–360 K.

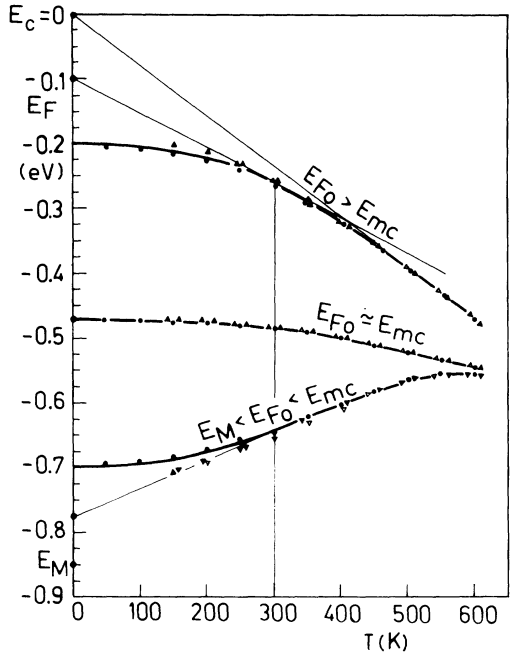

FIG. 2. Fully numerical $E_F(T)$ profiles (continuous lines) compared with points calculated under various approximations: (●) Boltzmann approximation (five-term equation) and root finder; (▲) three-term implicit equation; (△) three-term explicit equation with $C(E_{F0})$, $M(E_{F0})$. The model parameters are $kT_c=-kT_{mc}=0.026$ eV, $E_V=-1.7$ eV, $E_M=-0.85$ eV, $N_C=N_V=10^{22}$ $cm^{-3}eV^{-1}$, and $N_{mc}=10^{14}$ $cm^{-3}eV^{-1}$, but only their ratio matters, ensured by $E_{mc}=-0.479$ eV.

Now we turn to the physics behind MNR, and explain the success of the Boltzmann approximation in accounting for it.

The quantitative analysis of the Fermi-level thermal shift, based on the fully numerical treatment and analytic explicit approximations, has shown that one can account for the MNR with such a shift, controlled by only two exponential segments of the DOS, corresponding to tail states and adjacent midgap-defect states. Two interesting questions remain open, however: (a) is the *two-slope configuration* the minimum necessary one for the MNR? (This brings us to the features of the Fermi-level shift within a single-exponential-slope DOS, or *one-slope configuration.*); (b) if a *two-slope configuration* is necessary, what are the parameter requirements for a certain MNR to appear?

The answer to the first question is obtained with the analytic expressions in Appendix A, and is illustrated by the qualitative Fig. 3, for the Fermi level on the conduction-band side of the midgap peak E_M.

The *one-slope configuration* solution offers satisfactory low-temperature approximation for the thermal shift of a

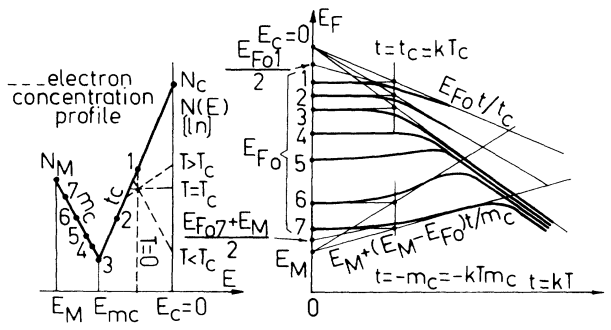

FIG. 3. The main $E_F(T)$ features resulting from the two-segment DOS model.

Fermi level situated at 0 K within an exponential segment of any DOS. The essential parameters for this solution are the following: (i) the characteristic energy associated with the logarithmic slope (t_c for points 1 and 2 and m_c for points 6 and 7 in Fig. 3), and (ii) the position at 0 K of the Fermi level with respect to the maximum value of the segment (E_C and E_M, for the tail segment and midgap segment, respectively). The temperature coefficient of E_F, located within an exponential segment falling from E_C towards the gap, is negligible around 0 K and then evolves, around a critical temperature T_c (associated with $t_c=kT_c$), towards a constant negative value proportional to E_C-E_{F0}.

But this proportionality does not result in the MNR in a temperature range well above T_c. The positive-slope condition $b>0$ imposed on Eq. (7) is not met and the activation energy of the conductivity E_σ^* is zero for all values of E_C-E_{F0}, as all curves extrapolate at $T=0$ to $E_F=E_C=0$ [$E_F^*=0$, according to Eq. (10)]. For a temperature equal to T_C, one has $E_\sigma^*=(E_C-E_{F0})/2$, and the temperature coefficient is proportional to E_σ^*, but again with a negative slope, and so MNR does not appear.

For an exponential segment falling from E_M towards E_C, similar results are obtained, with $-m_c, -T_{mc}$, and $E_{F0}-E_M$ playing the role of t_c, T_c, and E_C-E_{F0}, respectively.

The conclusion is therefore reached that *one-slope solutions cannot account for the MNR*. But it will be shown in Sec. III of this paper that they correspond to the negative-slope regions of the $\gamma^*(E_\sigma^*)$ dependence appearing in OT calculations for E_σ^* under 0.2 eV or above 0.8 eV.

In order to yield the positive-slope region, i.e., MNR, in the Fermi-level shift, the contributions of two exponential segments of the DOS should interact, resulting in a transition from having one prevailing in the shift, to the other. This condition is fulfilled by E_{F0} values illustrated with points 3–6 in Fig. 3. For temperatures around $T_C, -T_{mc}$, the corresponding $E_F(T)$ curves in Fig. 3 are well approximated by Eq. (7), MNR appears, and this fully settles the first question posed above.

The second question posed above will be fully answered in Sec. III. We will just mention here that even if *one-slope* ranges do not account for the MNR, their extent (minimum and maximum values reached by γ^*) controls the quantitative extent of the MNR range (positive $d\gamma^*/dE_\sigma^*$).

Before proceeding further with the MNR analysis, we make one more comment related to the characteristic energies (and temperatures) of exponential segments of the DOS. The equations in Appendix A, and Fig. 3 show that, for the Fermi level within such a segment, significant changes in the occupancy of the states appear around $T=T_c$. While at low temperatures an occupancy maximum and significant space charge appear close to the Fermi level, around T_c they move further, towards the highest end of the exponential segment. At $T=T_c$, the electron concentration profile is constant at energies above E_F.

Now, the physical reason for the success of the Boltzmann approximation in the evaluation of a significant thermal shift of the Fermi level, for exponential DOS profiles, becomes obvious: (i) at low temperatures, where significant space charge is around Fermi level, the latter remains in close proximity to E_{F0}; (ii) only around and above the characteristic temperature $T=T_c$ the Fermi-level shift becomes significant, being then controlled by space charge far from its position.

III. $N(E)$ DEPENDENCE OF THE MEYER-NELDEL PARAMETERS

The above-mentioned physical considerations are supported by the parametric equations of the dependence $\gamma^*(E_\sigma^*)$, with parameter E_F, which can be obtained through straightforward differentiation of Eq, (10) with respect to kT,

$$\gamma^*(E_F)/k=k^{-1}dE_F/dT=-[\bar{E}(E_F)-E_F]/kT\ , \quad (14)$$

with

$$\bar{E}(E_F)=E_F^*(E_F)=\frac{\int_{-\infty}^{+\infty}EN(E)f'((E-E_F)/kT)dE}{\int_{-\infty}^{+\infty}N(E)f'((E-E_F)/kT)dE}\ , \quad (15)$$

and

$$E_\sigma^*(E_F)=E_C-E_F^*(E_F)=E_C-\bar{E}(E_F)\ . \quad (16)$$

A general equation can also be obtained for the MNR slope, related to the slope of the dependence $\gamma^*(E_\sigma^*)$,

$$1/kT_{MN}=d(\gamma^*/k)/dE_\sigma^*=(1/kT)[1-(dE_F^*/dE_F)^{-1}]\ , \quad (17)$$

which gets close to $1/kT$ when $|dE_F^*/dE_F|\gg 1$. We can now examine the physical meaning of an activation energy, given by Eq. (12), which is significantly different from E_C-E_{F0}. The analytic expressions in Appendix A show—and Fig. 3 illustrates—that E_F^*, the extrapolation energy for the linear approximation, is close to E_{F0} only at low temperatures, and then it evolves towards E_C, passing through the value $(E_C-E_{F0})/2$ at $T=T_c$.

Equations (15) and (16) show that E_F^* and E_σ^* are both related to $\bar{E}_F$, the momentum of the electron-concentration variation, a kind of dominant energy for space-charge accumulation. At temperature T_c, for which the charge is uniformly distributed within the tail, $E_F^* = \bar{E}_F$ is not a dominant energy but just the middle of the energy range within which the charge is constant. The evolution of E_σ^* from $E_C - E_{F0}$ to zero is similar to that for the usual extrinsic conduction when the conduction-band edge becomes the dominant energy for charge-carrier density, which is temperature independent.

For the exponential profile of DOS given by Eq. (A1) (Fig. 7) reduced to a *two-slope* one and the Boltzmann approximation for the occupancy function, explicit parametric equations are given in Appendix B.

Figures 4(a) and 4(b) show calculated normalized curves $\gamma^*(E_{F0}^*)$, respectively, for flat and peaked distributions of the midgap states. The conclusion which can be drawn is that a simple DOS, with only two exponential segments, can quantitatively account, by use of various analytic expressions, for all kinds of $\gamma^*(E_\sigma^*)$ obtained by Overhof and Thomas.[14].

The curves in Figs. 4(a) and 4(b) show that the *two-slope* MNR range (positive $d\gamma^*/dE_\sigma^*$) is just a transition between tail and midgap *one-slope* ranges. The transition character is brought out even more clearly in Fig. 8 in Appendix B, which shows the dependence of E_{F0}^* (or $-E_\sigma^*$ for $E_C = 0$) on E_F. The slope dE_{F0}^*/dE_F in the transition range determines [through Eq. (17)] the deviation from kT of the MNR slope kT_{MN}.

As Fig. 4(a) suggests, a significant MNR range is expected only in the temperature range around and above the tail characteristic temperature T_c. It increases when tail-midgap transition energy gets deeper into the gap, and when midgap peak is more pronounced ($-T_{mc}$ as compared to T_c).

For a given tail, the most significant condition is $T = T_c$, under which very simple approximate expressions can be deduced (Appendix B), which correlate the DOS and MNR parameters. Some of these expressions are illustrated by characteristic limit lines in Figs. 4(a), 4(b), and 8. Perhaps the most interesting result is that the natural logarithm of the ratio between the extrapolation conductivity σ_{00} and Mott conductivity σ_m is around E_{mc}/kT_c.

Figure 5 illustrates the dependence on DOS parameters of the MNR correlation parameters, under some of the most favorable conditions for the latter to appear, $T = T_c = -T_{mc}$. Deviations from the dashed limit lines in Fig. 5 increase under $T < T_c$ and $T_c < -T_{mc}$ conditions.

We note that, in order to deduce correctly Mott's minimum-metallic-conductivity value from data on the temperature dependence on the conductivity with Meyer-Neldel correlation, one has to consider some additional information on DOS parameters, as well as *one-slope* regions of the $\gamma^*(E_\sigma^*)$ dependence, whenever possible.

Figure 6 is in the same format as OT's Fig. 8.5 in Ref. 14. It shows that experimental results on MNR, and the curve calculated by OT for a σ_m value of 150 $\Omega^{-1}\,\mathrm{cm}^{-1}$, are fully compatible with σ_m values between 15 and 1500 $\Omega^{-1}\,\mathrm{cm}^{-1}$, provided that the tail-midgap-state transition energy E_{mc} and midgap-state parameters E_M and T_{mc} are judiciously chosen. But important information may also be given by the MNR slope, which decreases (T_{MN} increases) when the fit is attempted for higher σ_m values.

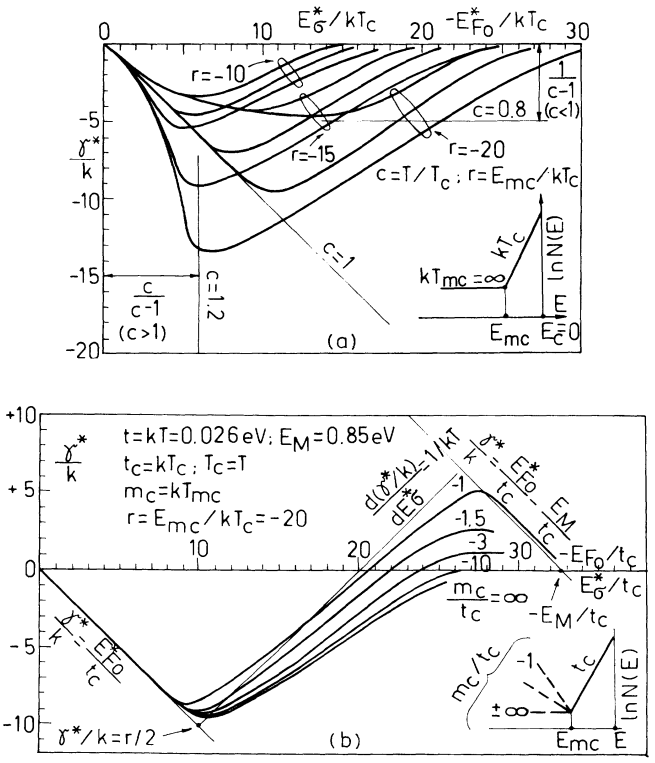

FIG. 4. Normalized dependencies γ^*/k on E_σ^*/t_c, for (a) flat midgap-defect-state profile and (b) peaked profile, and various normalized model parameters.

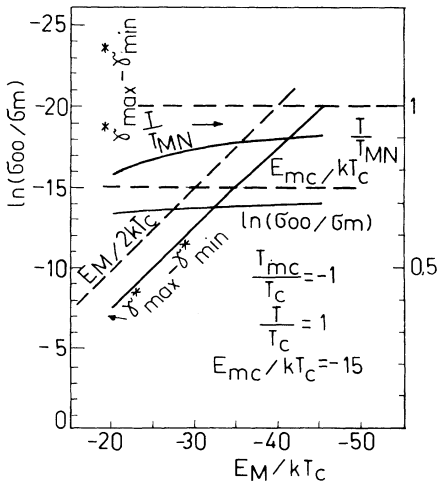

FIG. 5. Midgap energy dependence of MNR parameters; $T = T_c = -T_{mc}$ case.

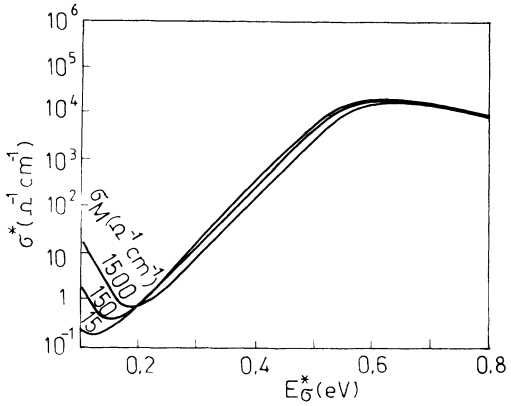

FIG. 6. MNR range, considered in Ref. 14, fitted respectively with $\sigma_m=15$, 150, and 1500 $\Omega^{-1}\,cm^{-1}$; $T/T_c=1.05$; $E_{mc}/kT_c=-11.2$, -13.5, and -15.8; $E_M/kT_c=-45$, -40, -33; $T_{mc}/T_c=-1.22$, -1.35, -1.8.

We will only mention here that the slightly higher slope of the OT-calculated curve, with respect to experimental data, might suggest that an underevaluated Mott's minimum-metallic-conductivity value has been used. But a more detailed exploration of DOS parameters would be needed to settle this matter. We will return to discuss these issues in a separate paper.

IV. CONCLUSIONS

We have shown that when one finds the Meyer-Neldel correlation within a certain temperature range, centered on a T value, one can safely assume that exponential tails of states, with a characteristic energy around kT, control the thermal shift of the Fermi level within that range. Such Meyer-Neldel tails also appear in doped single crystals, where they account for transitions involving levels far from the quasi-Fermi-level.[16,17]

When MNR is present, use of the dominant-energy approximation should be carefully reconsidered, if analytic treatment and experimental data processing are performed, because it may not be valid for some temperatures and the states around the Fermi level may not play a major role. Fully accounting for MNR parameters in terms of DOS parameters also allows for more reliable information to be obtained on Mott's minimum metallic conductivity.

ACKNOWLEDGMENTS

The support of the Department of Science and Education of Romania is acknowledged. Thanks are also due to Professor H. K. Henisch (Penn State University) for encouragement and support, which made this work possible, and to the Humboldt Foundation for help with computing equipment.

APPENDIX A

The exponential DOS profile, which essentially accommodates OT-type DOS, is shown in Fig. 7, and is characterized by the equations

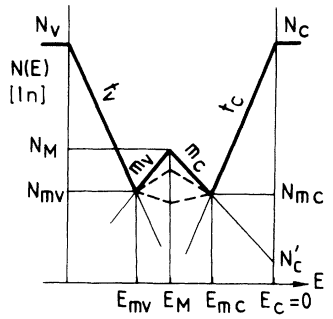

FIG. 7. The exponential profile of DOS used as a model.

$$N(E)=N_C \quad \text{for } E_C>E_C=0\ , \tag{A1}$$

$$\begin{aligned} N(E)=N_c(E)&=N_M\exp[(E-E_M)/m_c]+N_C\exp(E/t_C)\\ &=N'_C\exp(E/m_c)+N_C\exp(E/t_c)\ ,\\ N'_C&=N_M\exp(-E_M/m_c)\ ,\quad E_M<E<E_C\ , \end{aligned} \tag{A2}$$

$$\begin{aligned} N(E)=N_v(E)&=N_M\exp[(E-E_M)/m_v]\\ &\quad+N_V\exp[(E-E_V)/t_v]\ ,\quad E_V<E<E_M\ , \end{aligned} \tag{A3}$$

$$N(E)=N_V \quad \text{for } E<E_V\ , \tag{A4}$$

in which $t=kT$, $t_c=kT_c$, $m_c=kT_{mc}$, $n_v=kT_{mv}$, where the absolute values of T_c, T_v, T_{mc}, and T_{mv} are characteristic temperatures for the exponential dependencies of the model.

The exponentials with t_c,t_v correspond to disorder tail states, while those with m_c,m_v correspond to deep localized defect states. The parameters m_c,m_v can be either positive or negative, with the case of $m_c=t_c$, $m_v=t_v$ corresponding to the absence of deep levels with a nature different from that of tail levels.

In order to compare fully numerical-procedure results with analytic approximations we have used, for the occupancy function $f(x)$ $[x=(E-E_F)/kT]$, either the full Fermi-Dirac function

$$f(x)=1/[1+\exp(x)] \tag{A5}$$

or a two-term approximation that ensures correct $f(0),f'(0)$,

$$f(x)=\begin{cases}\exp(-x)-\frac{1}{2}\exp(-3x/2)\ , & x\geq 0\ ,\\ 1-\exp(x)+\frac{1}{2}\exp(3x/2)\ , & x<0\end{cases} \tag{A6}$$

or a Boltzmann approximation

$$f(x)=\begin{cases}\exp(-x)\ , & x\geq 0\ ,\\ 1-\exp(x)\ , & x<0\ ,\end{cases} \quad \text{satisfactory for } 1\times 1>3\ . \tag{A7}$$

When Fermi-Dirac $f(x)$ is replaced through the mentioned two-term approximation, the integral in Eq. (13)

can be analytically evaluated and split into 18 terms containing exponentials, out of which 10 correspond to the Boltzmann approximation of $f(x)$. One can now combine this analytical integration with the root-finder procedure and compare results with the full numerical procedure, and they nearly coincide even if only Boltzmann terms are retained.

Now, for the Boltzmann approximation and conditions imposed on $N(E)$ by OT (sufficiently high ratio between N_C, N_V and N_{mc}, N_{mv}, N_M), only five terms remain significant (for electron conduction) in Eq. (13), which reduces to

$$G(E_F) \cong Q - N_M M \exp[(E_M - E_F)/t] + N_C C \exp(E_F/t) - N_V V \exp[(E_V - E_F)/t] + N_C' O \exp(E_F/t) = 0 \ . \tag{A8}$$

The first term corresponds to the charge associated with the Fermi level sweeping the states, and the following three to the charge redistributed in deep states (m_c), conduction- (t_c), and valence-(T_v) band tails. The last term represents a correction to the charge around the Fermi level, with a significant contribution only when $|m_c| \gg t_c$, $N_M = N_C'$, (flat midgap profile).

The symbols Q, M, C, V, and O are given by the equations

$$Q = N_C t_c [\exp(E_F/t_c) - \exp(E_{F0}/t_c)] + N_M m_c \{\exp[(E_F - E_M)m_c] - \exp[(E_{F0} - E_M)/m_c]\} \ , \tag{A9}$$

$$C = t_c'[1 - \exp(E_F/t_c')] + t \ , \quad 1/t_c' = 1/t_c - 1/t \ , \tag{A10}$$

$$M = m_c''\{1 - \exp[(E_F - E_M)/m_c'']\} + m_v'' \ , \quad 1/m_c'' = 1/m_c - 1/t \ , \quad 1/m_v' = 1/m_v + 1/t \ , \tag{A11}$$

$$V = t_v''\{1 - \exp[E_M - E_V)/t_v'']\} + t \ , \quad 1/t_v' = 1/t_v + 1/t \ , \tag{A12}$$

$$O = m_c'[1 - \exp(E_F/m_c')] \ , \quad 1/m_c' = 1/m_c - 1/t \ . \tag{A13}$$

The parameters t_c', m_c', m_c'', and m_v'', help demonstrate that significant changes in the occupancy of the states appear around $T = T_c$, $T = -T_{mc}$, and $T = -T_v$.

Quantitatively exploring Eq. (A8), one finds not only that it gives practically the same results as the fully numerical procedure (Fig. 2) but that $E_F(T)$ behaviors, which result in MNR, are controlled, within the temperature range of interest, by the first three terms of the equation. This means that only the two exponential slopes of the DOS, which are close to the band prevailing in conduction (in our case conduction band) are significant for MNR.

Reduced to its first three terms, Eq. (A8) can be rewritten as a simple quadratic equation, with the solution,

$$\exp(E_F/t) \cong -(Q/2N_C C) \times \{1 \mp [1 + (4N_C N_M C M/Q^2) \times \exp(E_M/t)]^{1/2}\} \ , \tag{A14}$$

which is only apparently an explicit one, as the symbols Q, C, and M are functions of E_F, Eqs. (A9)–(A13). But a closer examination of Eq. (A9) shows that the dependence of the space charge Q on E_F is either negligible or only linear, with an insignificant effect on the solution within the range of interest. When significant for $E_F(T)$, the charge Q is essentially dependent only on E_{F0}, and can be approximated by Q_0, which is given only by the terms with E_{F0} in Eq. (A9).

As a consequence, Eq. (A14) can be used for fast approximate evaluation of $E_F(T)$ dependence, through an iterative procedure,

$$E_{Fi} = E_F(t_i, Q_0, C(E_{Fi-1}), M(E_{Fi-1})) \ , \tag{A15}$$

starting from $T, t = 0$ for which $E_F = E_{F0}$.

Depending on the E_{F0} position with the *two-slope* DOS, there are situations when Eq. (A8) reduced to only two terms: (i) when the space charge around E_{F0} is balanced only by the space charge in the same DOS segment as E_{F0} (*one-slope* behaviors); (ii) when the space charge redistributed within the two DOS segments balance each other, with space charge around E_{F0} having a negligible effect.

Two-term approximations allow for very simple equations to be written in such cases for $E_F(T)$, which allow for the simple and clear picture of this dependence, qualitatively illustrated in Fig. 3 for various situations. The equations demonstrate the significance of the characteristic temperatures T_c and $-T_{mc}$, through the expressions $C(E_F)$ and $M(E_F)$. The latter control E_F behavior under $T_c, -T_{mc}$, keeping it close to E_{F0}, then have more than an insignificant contribution, as E_F further moves only to keep the space charge constant at E_C or E_M.

As a consequence, one can write explicit approximate expressions for $E_F(T)$ that use the limit $C(E_{F0})$, $M(E_{F0})$ values. For E_F controlled only by tail states (points 1 and 2 in Fig. 3) one has

$$E_{F(T)} = E_{F0} T/T_c - kT \ln[C(E_F)/(kT_c)] \ , \quad C(E_F) \cong C(E_{F0}) \ , \tag{A16}$$

with kink temperature $T = T_c$, independent of E_{F0}.

For E_F controlled only by midgap states (points 6 and 7 in Fig. 3),

$$E_F(t) = E_M + (E_M - E_{F0})T/T_{mc} + kT \ln[-M(E_F)/(kT_{mc})] \ , \quad M(E_F) \cong M(E_{F0}) \ , \tag{A17}$$

with kink temperature $T = -T_{mc}$, independent of E_{F0}. For E_F controlled by tail and flat midgap states ($|m_c| \gg t_c$),

$$E_F(T) = E_{F0} - (t_c' + t)\exp[E_F/kT - E_{F0}/kT_L] \ , \quad T_L = T_c E_{F0}/E_{mc} \ , \tag{A18}$$

with the kink temperature at T_L, proportional to E_{F0}.

The approximations $C = C(E_{F0})$ and $M = M(E_{F0})$ can also be used in Eq. (A14), which becomes an explicit one,

still giving satisfactory results in evaluating $E_F(T)$ over the range of interest for MNR, as shown in Fig. 2.

APPENDIX B

For a *two-slope* DOS and Boltzmann approximation, Eq. (A8) can be rewritten in the following form, convenient for the MNR range, i.e., temperatures around and above T_c:

$$G(E_F)\cong Q+N_C' t\bar{M}\exp(E_F/m_c)-N_C t\bar{C}\exp(E_F/t_c) + N_C' t\bar{O}\exp(E_F/m_c)\ , \tag{B1}$$

with the symbols $\bar{C}$, $\bar{M}$, and $\bar{O}$, given by the expressions

$$\bar{C}=t_c'[1-\exp(-E_F/t_c')]/t\ , \tag{B2}$$

$$\bar{M}=m_c''\{1-\exp[(E_M-E_F)/m_c'']\}/t\ , \tag{B3}$$

$$\bar{O}=m_c'[1-\exp(-E_F/m_c')]/t\ . \tag{B4}$$

By differentiating Eq. (A1) with respect to temperature, and also using for convenience the symbols

$$G=t_c'[\bar{C}t/E_F-\exp(-E_F/t_c')]/t\ . \tag{B5}$$

$$W=m_c''\{\bar{M}t/(E_F-E_M)-\exp[(E_M-E_F)/m_c'']\}/t\ , \tag{B6}$$

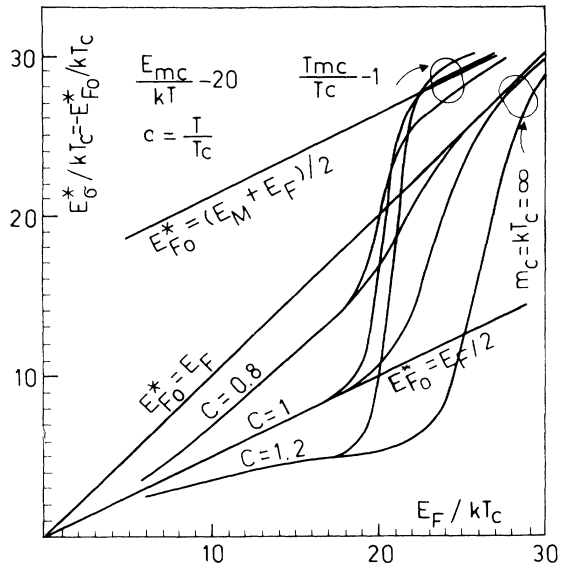

FIG. 8. The normalized dependence E_σ^*/kT_c on E_F/kT_c.

$$U=m_c'[\bar{O}t/E_F-\exp(-E_F/m_c')]/t\ , \tag{B7}$$

one obtains the parametric equations of the $\gamma^*(E_\sigma^*)$ dependence,

$$\gamma^*(E_F)=\frac{(GE_F/t)\exp[(E_F-E_{mc})/t_c]+[UE_F/t+W(E_M-E_F)/t]\exp[(E_F-E_{mc})/m_C]}{\bar{C}\exp[(E_F-E_{mc})/t_c]+(1+\bar{O}-\bar{M})\exp[(E_F-E_{mc})/m_c]}\ , \tag{B8}$$

$$E_\sigma^*(E_F)=E_C-E_F^*(E_F)\ ,\quad E_F^*(E_F)=E_F-t\gamma^*(E_F)\ . \tag{B9}$$

Equations (B8) and (B9) have been used to calculate normalized dependencies between γ^*/k and E_{F0}^*/t_c, in Figs. 4(a) and 4(b), and the curves $\sigma_0^*(E_\sigma^*)$ in Fig. 6. Equation (B8) has also been used to calculate curves in Fig. 8.

This figure, as well as Fig. 3, shows that MNR is due to significant changes in E_σ^* (or E_{F0}^*), and the slope of $E_F(T)$ dependence, which appear for small changes in E_{F0} around the E_{mc}, the tail-midgap transition energy in the DOS.

[1]N. F. Mott, Philos. Mag. B **43**, 941 (1981).

[2]J. Stuke, in *Proceedings of the Third International Conference on Amorphous and Liquid Semiconductors, Cambridge, England, 1969,* edited by Sir Nevill Mott (North-Holland, Amsterdam, 1970), p. 1.

[3]I. Solomin, J. Dietl, and D. Kaplan, J. Phys. (Paris) **39**, 1241 (1978).

[4]J. Tardy and R. Meaudre, Solid State Commun. **39**, 1031 (1981).

[5]R. Meaudre, Philos. Mag. B **51**, L57 (1985).

[6]W. Rehm, R. Fischer, J. Stuke, and H. Wagner, Phys. Status Solidi B **79**, 539 (1977).

[7]D. E. Carlson and C. R. Wronski, in *Amorphous Semiconductors,* edited by M. H. Brodsky, Topics in Applied Physics Vol. 36 (Springer, Berlin, 1979), Chap. 10.

[8]W. E. Spear, D. Allen, P. G. LeComber, and A. Ghaith, Philos. Mag. B **41**, 419 (1980).

[9]H. Fritzche, Sol. Energy Mater. **3**, 447 (1980).

[10]W. Meyer and H. Neldel, Zh. Tekh. Fiz. **12**, 588 (1937).

[11]F. Djamdji and P. G. LeComber, Philos. Mag. B **56**, 31 (1987).

[12]R. Schumacher, P. Thomas, K. Weber, W. Fuhs, F. Djamdji, P. G. LeComber, and R. E. I. Schropp, Philos. Mag. B **58**, 389 (1988).

[13]H. Overhof and W. Beyer, Philos. Mag. B **43**, 433 (1981).

[14]H. Overhof and P. Thomas, in *Electronic Transport in Hydrogenated Amorphous Semiconductors,* edited by G. Hohler,

Springer Tracts in Modern Physics Vol. 114 (Springer-Verlag, Berlin, 1989), pp. 41, 43, 126, and 128.
[15]P. Irsigler, D. Wagner, and J. Dunstan, J. Phys. C **16**, 6605 (1983).
[16]P. Eliseev, A. I. Krasilnicov, M. A. Manko, and I. Z. Pinsker, Phys. Status Solidi **23**, 587 (1967).
[17]A. Goldenblum, Rev. Roum. Phys. **17**, 81 (1972).